RESEARCH ARTICLE

NANO · MICRO small
www.small-journal.com

Evidence for *Trans*-Oligoene Chain Formation in Graphene Induced by Iodine

*Fabian Grote, Benjamin I. Weintrub, Mira Kreßler, Qing Cao, Christian E. Halbig, Patryk Kusch, Kirill I. Bolotin, and Siegfried Eigler**

Functionalization of pristine graphene by hydrogen and fluorine is well studied, resulting in graphane and fluorographene structures. In contrast, functionalization of pristine graphene with iodine has not been reported. Here, the functionalization of graphene with iodine using photochemical activation is presented, which is thermally reversible at 400 °C. Additional dispersive dominant Raman modes that are probed by resonance Raman spectroscopy are observed. Additionally, iodinated graphene is probed by Kelvin probe force microscopy and by transport measurements showing p-doping surpassing non-covalent iodine doping by charge transfer-complex formation. The emergent Raman modes combined with strong p-doping indicate that iodine functionalization is distinct from simple iodine doping. A reaction mechanism based on these findings is proposed, identifying the large size of iodine atoms as the probable cause governing regiochemically controlled addition due to steric hinderance of reactive sites. The modification of the electronic structure is explained by the confinement of 1D *trans*-oligoene chains between sp^3-defects. These results demonstrate the uniqueness of iodine reactivity toward graphene and the modification of the electronic structure of iodinated graphene, highlighting its dependence on the spatial arrangement of substituents.

1. Introduction

Pristine graphene is highly inert and requires harsh reaction conditions to form additional out-of-plane chemical bonds for developing advanced post-functionalization strategies.[1] Efficient methods have been developed to achieve the controlled functionalization of pristine graphene,[2] such as strong n-doping by alkali metals enabling the reaction with electrophiles, for example, diazonium ions or alkylhalides.[3] Another approach relies on cycloaddition reactions, for example with azido compounds.[4] Radical addition reactions have been widely used in graphene functionalization with hydrogen, oxygen,[5] halogens, alkyl, nitrenes, and phenyl groups.[2,6] However, they often require activated graphene, for example by defects. Therefore, reduced graphene oxide is often used as a defect-activated graphene starting material. In earlier studies, we demonstrated that organic and hydroxyl radicals preferentially react close to defect sites and thus, defects guide the regiochemical addition of addends.[7] Among the functionalization reactions of pristine graphene hydrogenation and fluorination have been widely studied. The syntheses of those materials typically require either preactivation by n-doping,[8] or high temperatures and highly reactive reactants such as fluorine or xenon difluoride making reaction control challenging.[9]

In contrast to the extensive reports of halogenation reactions including chlorine and bromine,[10] there is, to the best of our knowledge, no example of iodination of high-quality graphene. Previous studies have reported the iodination of graphene but using reduced graphene oxide as starting material, where the reactivity is dominated by defects.[11] Li et al. investigated the electrochemical iodination of graphene and found no reaction of iodine radicals with graphene but reported deposition of molecular iodine instead. This was explained by the lower reactivity of iodine radicals compared to other halogen radicals.[12] In addition to the bare halogenation reaction of graphene, the substantial van der Waals radius of iodine radicals (198 pm[13]) should result in distinctive regiochemical control of addition patterns on graphene[14], besides the most stable 1,2-addition.[15] However, thus far, only a few Raman studies have hinted at the existence of such reactivity, with minor Raman bands being reported for arylated graphene[16] and a few more accounts of similar modes can be found, which were assigned to *trans*-polyacetylene chain formation.[17] Similar signals in chlorinated graphene have been assigned to doping-activated Raman modes, making the

F. Grote, Q. Cao, C. E. Halbig, S. Eigler
Institut für Chemie und Biochemie
Freie Universität Berlin
Altensteinstraße 23a, 14195 Berlin, Germany
E-mail: siegfried.eigler@fu-berlin.de

B. I. Weintrub, M. Kreßler, P. Kusch, K. I. Bolotin
Institut für Physik
Freie Universität Berlin
Arnimallee 14, 14195 Berlin, Germany

The ORCID identification number(s) for the author(s) of this article can be found under https://doi.org/10.1002/smll.202311987

DOI: 10.1002/smll.202311987

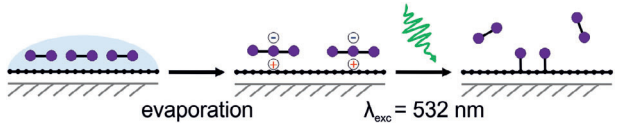

Figure 1. Schematic illustration of the iodination process. A solution of iodine in methanol is deposited on graphene supported on SiO_2/Si substrate. Upon evaporation of methanol, polyiodides I_3^- and I_5^- form by charge-transfer complex formation. Irradiation of this complex with λ_{exc} = 532 nm forms iodine radicals (Equation 1) that react with the graphene and excess iodine evaporates.

origin of these signals disputed.[18] Scanning tunneling microscopy (STM) experiments of hydrogen radicals on graphene allowed direct observation of effects of addition patterns on graphene properties.[19] Additionally, DFT calculations suggest considerable influence of the addition patterns on electronic and magnetic properties (e.g., bandgap opening).[20] To date, a lack of insight into possible reaction mechanisms prohibits the rational design of regular addition patterns on 2D materials.

Here, we present a novel approach to photochemically iodinate defect-free graphene after doping with polyiodides (**Figure 1**). We observe new dispersive Raman signals with unprecedented intensity and a strong p-doping effect measured by transport measurements, X-ray photoelectron spectroscopy (XPS), and Kelvin probe force microscopy (KPFM), that exceeds iodine doping. A reaction mechanism is proposed to explain the observed properties, in which steric hinderance of reactive sites due to the large iodine atom size forms well-defined addition patterns of *trans*-oligoene chains between sp^3-defects.

2. Results and Discussion

In this study, we used single-layer graphene obtained either by tape exfoliation or by chemical vapor deposition (CVD). With those approaches we ensure high quality of graphene to exclude dominant effects of pre-existing defects or residues from the fabrication process on the iodination reaction (Figure 1). To mitigate the influence of the substrate, we deposited monolayers of graphene on SiO_2, Au, and h-BN, respectively (Figure S1, Supporting Information). The graphene structures were thermally annealed (T = 200 °C, $p = 1 \times 10^{-3}$ mbar, 2 h) to ensure stable adhesion of graphene to the substrate and to remove volatile impurities. Before inducing the iodination reaction, the density of defects was quantified by Raman spectroscopy.

First, we deposited iodine onto graphene from a methanol solution (20 mM$_M$), leading to p-doping of graphene and polyiodide formation.[11a,21] After evaporation of methanol at room temperature, the doped graphene was iteratively irradiated using the laser of the Raman microscope (λ_{exc} = 532 nm, 3.03 mW, 30 accumulations). The Raman spectrum (**Figure 2**, purple spectrum) of iodinated graphene features two new dominant Raman modes at 1115 and 1498 cm^{-1}, while no new signals are observed on the substrate. This excludes reactions with the substrate or adsorbates as the cause of these signals. The observed signals were persistent after evaporation of iodine in a vacuum (T = rt, $p = 1 \times 10^{-3}$ mbar, 16 h) and washing with water or alcohols that should remove any non-covalently bound iodine. To gain further insights into the proceeding reaction, we elucidated the reaction mechanism, focusing our attention on the iodine species.

Polyiodides I_3^- and I_5^-, detected by Raman spectroscopy at 107 and 162 cm^{-1} (Figure S2, Supporting Information) are observed exclusively on graphene while no polyiodide signals are detected on the substrate. The doping effect is apparent by the shift of the G-peak by up to 15 cm^{-1} (Figure S2, Supporting Information) and partial 2D-peak suppression.[22] When iodine-doped graphene is irradiated with λ_{exc} = 532 nm, iodine radicals $I^\bullet$ and $I_2^{-\bullet}$ are generated through the photodissociation of I_3^- and I_5^- anions, as shown by Gardner et al. (Equation 1).[23]

$$I_3^- \xrightarrow{h\nu} [I_3^-]^* \rightarrow I_2^{-\cdot} + I^\cdot \quad (1)$$

The $I_2^{-\bullet}$ radical can further dissociate into an $I^\bullet$ radical and iodine anion.[13] While the photoredox chemistry of polyhalides is widely studied in metal halide complexes, examples on the photochemistry of halides at the surface of 2D materials are rare.[18a,24] The nascent radicals near the graphene surface subsequently react with sp^2-carbon atoms to form carbon-iodine bonds. Throughout this manuscript we will refer to the product of this reaction as "iodinated graphene" without distinction between tape-exfoliated and CVD graphene since we did not find a difference for the reactivity of the starting materials. Although only triiodide and pentaiodide are directly observed in the Raman spectra, higher polyiodides could form a network on the graphene surface.[25] To the best of our knowledge this is the first time that a photochemical reaction of a polyhalide and graphene is described. In contrast to the common evolution of Raman spectra of functionalized graphene,[26] the G/2D-ratio increases from 0.52 to 0.92 indicating increased disorder in the graphene lattice (Figure 2), however, no D-peak at ≈1340 cm^{-1} is observed.

Signals with smaller intensity evolve (ν_2, $2\nu_1$, and $\nu_1+\nu_3$, Figure 2), of which a detailed description can be found in the SI (Figure S3A, Supporting Information). The lack of a D-peak

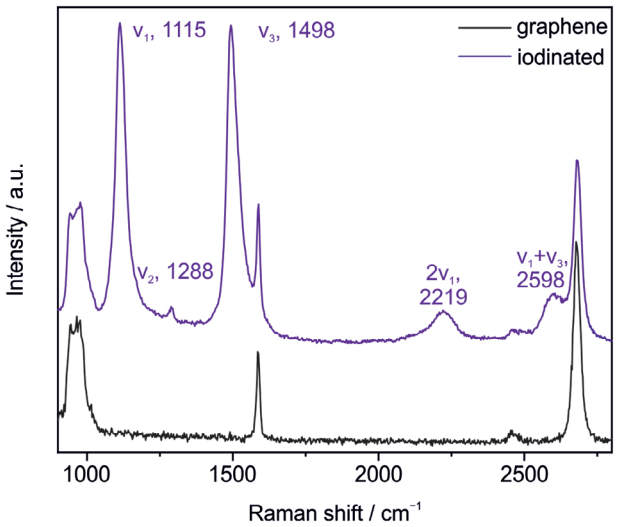

Figure 2. Raman spectrum (λ_{exc} = 532 nm) of tape-exfoliated graphene on SiO_2/Si before (black) and after iodination (purple). Two strong new modes (ν_1, ν_3) and three smaller modes (ν_2, $2\nu_1$, and $\nu_1+\nu_3$) are observed in the same range.

either indicates absence of functionalization or formation of Raman silent defects, as reported, for example, for zigzag edges, charged impurities, and intercalants.[27]. Raman probing iodinated samples with λ_{exc} = 638 nm (1.94 eV) shows dispersion of the new Raman modes and a strong change in the intensity relative to the graphene signals (**Figure 3A**). At higher excitation energies (λ_{exc} = 405 nm, 3.06 eV) no Raman modes were observed, while the signal intensities measured at longer wavelengths were shifted after irradiation due to defunctionalization (Figure S5A, Supporting Information). Surprisingly, in some areas of the sample, using the same reaction conditions, the G- and 2D-peaks typical for graphene completely vanish, indicating the formation of a new material (Figure 3B). A strong increase of the photoluminescence background is observed and formation of two strong new signals at 1121 and 1504 cm^{-1} that show a striking similarity to *trans*-polyacetylene (Table S1, Supporting Information). *Trans*-polyacetylene has two strong modes at 1125 and 1512 cm^{-1} (upon irradiation with λ_{exc} = 532 nm[28]) and a similar pattern of signals and overtones.[29] It also shows resonance Raman effects due to the chainlength-dependent bandgap and a large Raman cross section leads to high intensities of the Raman modes (Figure S4A, Supporting Information).[30] The Raman results therefore suggest a structure like *trans*-polyacetylene polymer (Figure S3B, Supporting Information). Those localized conjugated double bonds may result from a regioselective addition reaction of large and sterically demanding iodine atoms to graphene. To distinguish the structures in iodinated graphene from *trans*-polyacetylene, where each carbon atom is bonded to a hydrogen atom, we refer to the chains we propose in iodinated graphene as *trans*-oligoene chains. These 1D carbon chains are bonded to carbon atoms within the graphene structure, have varying finite lengths and are spread randomly across the iodinated graphene area with an unknown distribution. While we expect different Raman signal positions between *trans*-polyacetylene and graphene-embedded *trans*-oligoenes, we expect to observe similar trends depending on the chain length due to bandgap opening.[31]

The reversibility of iodination reactions is of special interest for patterning applications, for example, for writing, reading, and erasing information.[18b] Thus, we investigated the thermal defunctionalization of iodinated graphene, which we find to occur between 150 and 400 °C. Interestingly, a thermal iodination of graphene occurs without irradiation, as identified by the appearance of similar but less intense Raman modes at 150 °C under ambient conditions (Figure S6, Supporting Information). After extended times of vacuum annealing at 200 °C, an increase of the new modes is observed that remain stable up to 300 °C. This may be due to iodine intercalated between graphene and the SiO_2 substrate that is unable to evaporate, and thus, the iodine can react with graphene.[21b] Heating of iodinated graphene to 400 °C removes the new modes and a broad D-peak at 1349 cm^{-1} (FWHM = 171 cm^{-1}) forms. Additionally, the base of the G-peak broadens, while the top remains sharp (Figure 3C). The broad D-peak is reminiscent of disordered carbon[32] and may originate from amorphous carbon on the graphene surface formed by graphitization of organic adsorbates from the environment.[33] Defunctionalization was also observed when high laser intensities were used, probably due to local heating or assisted photochemical bond dissociation, shifting the distribution of *trans*-

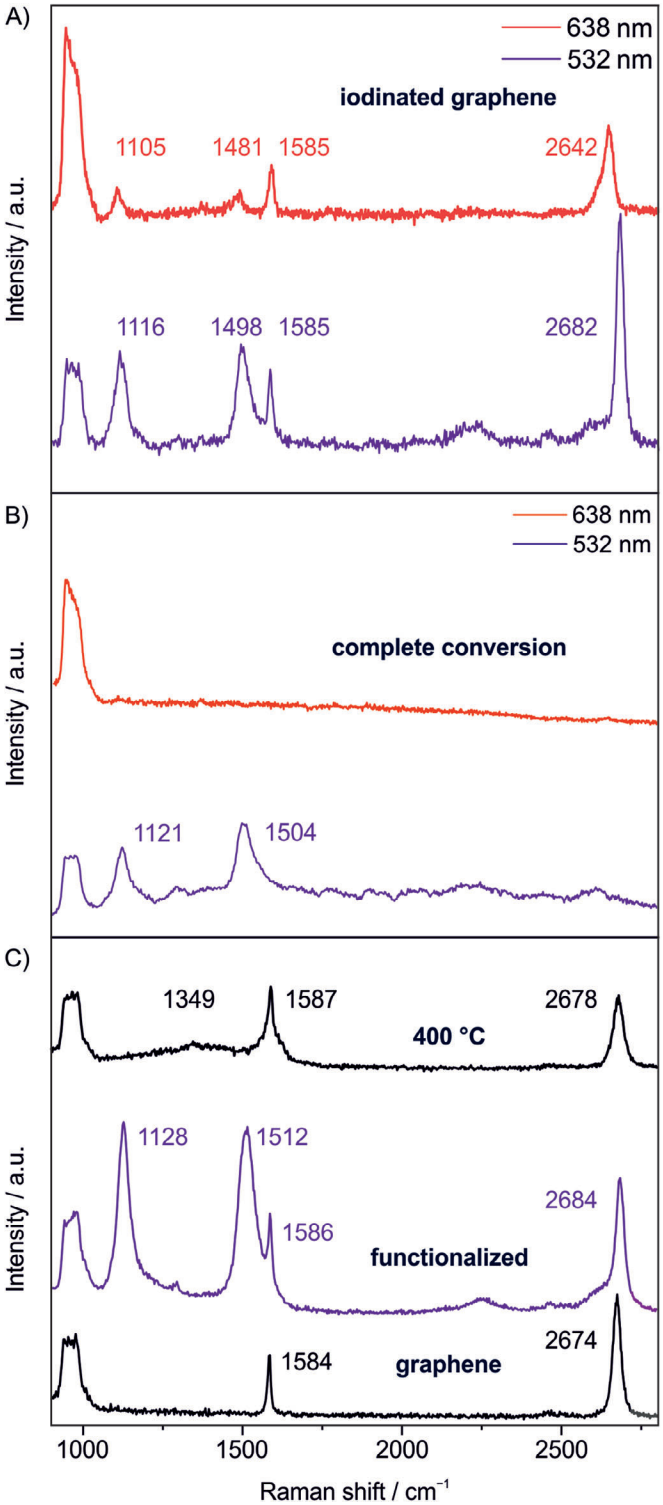

Figure 3. A) Raman spectra of tape-exfoliated graphene on hBN/SiO_2/Si after iodination measured at 532 nm (purple) and 638 nm (red), showing signal dispersion and a strong decrease of intensity relative to the graphene signals. B) Example spectra of vanished graphene Raman modes. No Raman signals are observed at 638 nm indicating the complete conversion of graphene. C) Raman spectra of pristine tape-exfoliated graphene, iodinated graphene, and graphene annealed at 400 °C. The graphene rests on a SiO_2/Si substrate.

oligoene chains (Figure S5B, Supporting Information). The high thermal stability indicates a thermodynamically stable structure.

With XPS the halogen content was determined and covalent bond formation of halogens to graphene was confirmed.[34] We functionalized CVD graphene on a large area (Figure S7A, Supporting Information) and thoroughly washed it (water, isopropanol, acetone) to remove all residues on the material before measurements. The survey spectrum (Figure S7B, Supporting Information) shows the characteristic I $3d_{5/2}$ and I $3d_{3/2}$ peaks at 619.5 and 630.5 eV respectively, but with very low signal intensities (Figure S7C, Supporting Information). The deconvolution of the C 1s signal shows no significant change of the carbon composition (Figure S7D, Supporting Information), as expected due to the small amount of iodine present. With respect to the intensity of the C 1s peak at ≈284.4 eV, we estimated the atomic ratio of iodine to carbon to be ≈1–300. Thus, deconvolution of the high-resolution C 1s and I 3d core spectra cannot provide further meaningful information due to the small signal-to-noise ratio in the present spectra. Hence C 1s core spectra of graphene before and after functionalization are practically similar (Figure S7D–F, Supporting Information).

Similar Raman signals emerge when graphene is irradiated under similar conditions with bromine instead of iodine (Figure S8D, Supporting Information). The larger difference of electronegativity between carbon and bromine should cause a stronger separation of XPS signals. We thermally brominated CVD graphene (Figure S9A, Supporting Information) to ensure homogenous functionalization across a large sample. The survey spectrum shows the characteristic Br 3d peak at 70 eV albeit with a low intensity (Figure S9B,C, Supporting Information) but the broadness of the bromine high resolution Br 3d core spectrum indicates the presence of C—Br bonds.[35] Deconvolution of the C 1s signal showed no significant change of the carbon composition, as expected from the low intensity of the bromine signals (Figure S9D, Supporting Information).

The introduction of semiconductive *trans*-oligoene chains and difference in electronegativity between carbon and iodine should cause p-doping of the iodinated graphene. To test this, we performed electrical transport measurements on graphene transistors before and after iodination. In contrast to Raman spectroscopy where we can only observe a small portion of the *trans*-oligoene chain distribution the entire system is probed in transport measurements. The carrier density of graphene for the transport measurements can be calculated using Equation 2, where n = carrier density, C = total areal capacitance, V_g = gate voltage, V_{CNP} = charge neutrality point, and e = elementary charge.

$$n = C\frac{(V_g - V_{CNP})}{e} \quad (2)$$

We find that pristine graphene has a carrier density of 0.9 × 10^{12} holes cm^{-2} (V_{CNP} = 11.5 V), probably due to the SiO_2 substrate as well as water and impurities trapped between graphene and the substrate.[36] Graphene exposed to gaseous iodine is also p-doped due to charge-transfer complex formation.[37] Measurements of iodine-doped graphene prepared by our process under ambient conditions showed decreasing doping levels during the measurement (≈30 min) due to its considerable vapor pressure and did not exceed 3.2 × 10^{12} holes cm^{-2} (V_{CNP} = 43 V), consistent with literature values (Figure S10C, Supporting Information). To minimize iodine doping effects in our device, we stored the samples under high vacuum conditions (≈10^{-5} mbar) for several hours to evaporate any leftover iodine from the functionalization process. Iodination strongly increased the hole density to 5.8 × 10^{12} holes cm^{-2} (V_{CNP} = 77 V, **Figure 4A**), corresponding to a Fermi energy difference of ΔE_F = 173 meV, exceeding doping levels from charge-transfer into polyiodide molecules. A significant hysteresis is observed for iodinated graphene that is distinct from the pristine or iodine-doped graphene. This may be explained by capacitive charging of trap states that are formed by the *trans*-oligoene chains.[38] In contrast to iodine-doped graphene, the carrier density was stable under vacuum conditions and over several gate voltage sweeps, since the covalently attached iodine is not removed in low pressure conditions (Figure S10D, Supporting Information). It is interesting to note that iodine functionalization induces a free carrier concentration in graphene close to the limit of conventional SiO_2 gating. Other halogenated graphene devices showed strong p-doping as well, however in these examples no V_{CNP} of the functionalized graphene were reported, due to the limited measurement window.[24,39] Calculating carrier densities is limited, since it relies on accurately extracting V_{CNP} from the transport curves, which is in some cases beyond the range of V_g values which could be applied without destroying the sample.

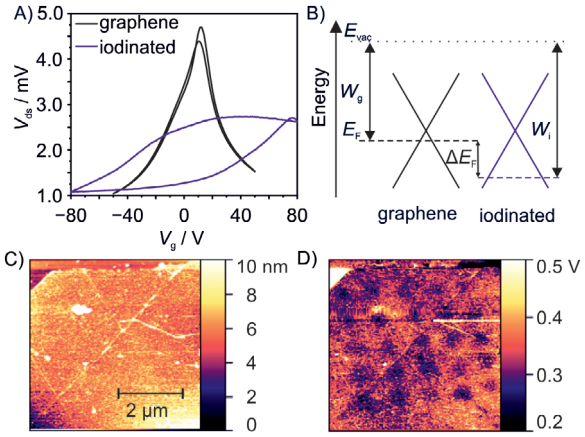

Figure 4. A) Drain-source voltage versus gate voltage of graphene field-effect transistor before (black) and after (purple) iodination. B) Energy level diagram of graphene and iodinated graphene. The Fermi energy (E_F) is significantly decreased upon iodination as evidenced by KPFM and transport data. C) Topography image of iodinated CVD graphene showing no signs of patterning. D) KPFM image of the same area. A 4 × 4 µm pattern was made by irradiation with λ_{exc} = 532 nm and 1 µm step size, visualized by black dots wihich indicate a lower work function relative to unfunctionalized areas.

Thus, we used KPFM as a complementary experimental method to measure local carrier density differences. The work function difference of pristine (W_g) and iodinated areas (W_i) directly corresponds to the difference of the Fermi level ($\Delta E_F = W_i - W_g$) of the two areas (Figure 4B). We measured KPFM on a graphene flake with both pristine and iodinated areas and compared the work functions between these areas to calculate a local work function difference. The topographic scan shows

no significant variation of sample height between pristine and iodinated areas (Figure 4C), but the overall height of the monolayer reveals the presence of adsorbates despite extensive washing (water, isopropanol, acetone) and evaporation in vacuum. If the material properties would result from adsorbates on the surface of graphene, differences in the intensity of the Raman and KPFM signals must be detectable between cleaned and uncleaned domains. To investigate this we measured Raman spectra and KPFM of the CVD graphene sample before (Figure 4C,D) and after (Figure S11D,E, Supporting Information) removal of adsorbates by mechanical cleaning with an AFM tip.[40] After cleaning of the graphene surface, the v_1 and v_3 mode remain unchanged in the cleaned areas while no change of Raman signal was observed for the piled adsorbates (Figure S11B,C, Supporting Information). Also, the work function patterns remain in the KPFM image (Figure S11E–I, Supporting Information), while the contrast between functionalized and unfunctionalized areas is improved due to the removal of adsorbates with a higher work function (Figure S11G,I, Supporting Information). No change of the Raman signals of brominated graphene (Figure S8C,D, Supporting Information) was observed after mechanical cleaning. The adsorbates therefore have no significant influence on the material properties and consequently, the new Raman modes must stem from the carbon lattice.

To extract a reliable work function difference, we prepared a tape-exfoliated graphene sample contacted with a gold electrode to ensure proper grounding (Figure S12A, Supporting Information). The sample was patterned, and the functionalization was followed by Raman spectroscopy (Figure S12B, Supporting Information). The average difference of the work function between pristine and iodinated areas measured by KPFM was 141.5 meV (Figure S12C–E and Table S2, Supporting Information). This is in good agreement with ΔE_F extracted from transport measurements (173 meV) considering that these two values are measured on different samples and by different techniques. The observed shift of E_F suggests that the carrier density changes by iodination exceed iodine doping and are stable against decay by iodine evaporation.

In an earlier report by Englert et al. small Raman modes at 1139 and 1512 cm^{-1} (λ_{exc} = 532 nm) were observed in the covalent functionalization of graphene with aryl radicals, similar to the v_1 and v_3 modes of iodinated graphene.[16] They assigned the observed modes to *trans*-oligoene chains formed within areas defined by sp^3-defects based on their similarity to Raman modes observed in nano-crystalline diamond samples.[30] Similar modes were observed upon photochlorination of graphene with chlorine gas; again with relatively low intensities.[18] They assigned the signals to effects of strong doping by chlorine addition leading to symmetry lowering and zone folding that activate new Raman modes by comparison to potassium-doped graphene (n-doped).[41] The modes observed in that system however are observed at 1134 and 1267 cm^{-1} while no signal ≈1500 cm^{-1} was observed that would account for the v_3-modes. Instead, a Fano-shaped G-peak is observed and such a mode is also not predicted by calculations of the Raman modes of KC_8.[42] If the observed Raman modes would arise from a doping effect, then they should evolve without irradiation of the sample and should be sensitive toward removal of the dopant by washing or evaporation. Interestingly, in other reports of chlorination of graphene, these spectral features were not reported.[12,24,43] We find that the spectral modes of the polyiodides vanish, while two strong new modes appear (Figure 2), which we would not expect for a non-covalent polyiodide network. The Raman modes of iodinated graphene are also persistent under ambient and high vacuum conditions or washing with water and organic solvents in contrast to the polyiodide signals. The complete disappearance of graphene Raman signals in some areas and the dispersive nature of the Raman modes indicate the direct interaction with the carbon lattice. Their unprecedented intensity allowed us to observe the v_2 mode and additional overtone modes that have not been reported for any functionalized graphene before and further indicate an origin from a *trans*-polyacetylene like structure. Their strong p-doping effect exceeds doping by non-covalently adsorbed polyiodides as shown by transport and KPFM measurements, and the weak doping effect of iodine makes doping-activated Raman modes appear unlikely.

We explain these experimental results by the formation of *trans*-oligoene chains formed with regiochemical control due to the large iodine size. Their formation depends on the reactivity of the iodine radical on the graphene sheet,[44] since the reaction of an iodine radical with graphene forms a π-radical that initially resides in a non-bonding orbital adjacent to the iodine addition site (**Figure 5**A). The delocalization of the π-radical was directly observed for hydrogenated graphene by STM causing a long-range modification of the local spin density of states and showing a threefold symmetry,[45] reaching as far as 6 nm or 20–25 lattice constants.[45] It corresponds to the delocalization of the π-radical on the B sublattice and can be interpreted as delocalization along the *trans*-oligoene paths shown in red in Figure 5B. The highest spin density, and therefore highest reactivity, is located on the three carbon atoms in 1,2-position adjacent to the addition site and at the 3 *cis*-1,4-positions (grey, Figure 5B) across six-membered rings[46] and the second hydrogen radical addition thus occurs at these positions, as observed experimentally.[15] The high reactivity of radicals may enable other addition patterns to form under kinetic control,[14] but here the low reactivity of iodine radicals is expected to lead to thermodynamic rather than kinetic reactivity. Equally important, addition in the 1,2-position is sterically blocked by iodine due to the large van der Waals radii of the iodine atoms (198 pm) and the resulting electrostatic repulsion.[13] The *cis*-1,4-addition motif (A, Figure 5C) leads to a separation of the iodine pair of 284 pm (assuming C—C bond distance of 142 pm), which is only slightly longer than the covalent bond length of diiodine (267 pm), making it also unlikely. By addition in the *trans*-1,4-position (B, Figure 5C) the defect distance is 376 pm, making a stable addition possible, explaining the observed regioselectivity. Since in our experiment the whole surface is covered with iodine, the second reaction step may be very fast and could potentially even extend beyond the irradiated area due to the delocalization of the π-radical on the graphene sheet. The confinement of localized double bonds between sp^3-defects induces bond length alternation through Peierls distortion, causing chain-length dependent local bandgap opening and hence resonance Raman effect.[47] A distribution of various chain lengths is formed that explains the varying intensities and dispersion of the Raman modes (Figures S4B and S5B, Supporting Information).

Up to three *trans*-oligoene chains may form from a single sp^3-defect, following the symmetry observed for the spin

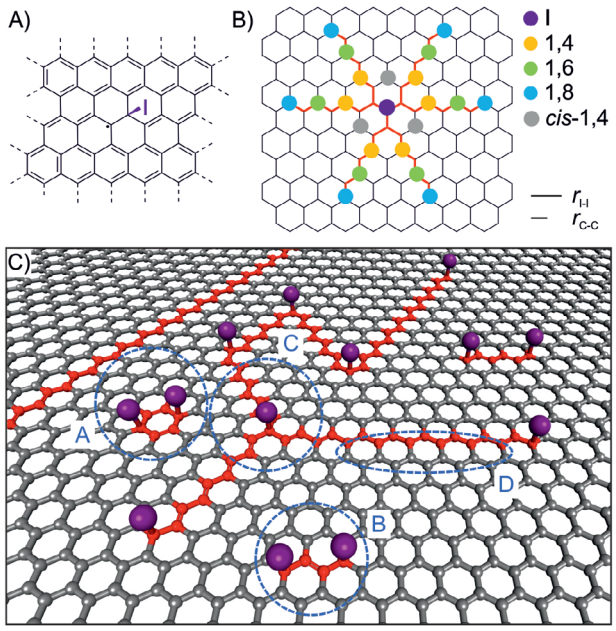

Figure 5. A) Addition of an iodine radical to graphene. The π-radical is located adjacent to the sp^3-defect and can be delocalized on the sublattice. B) Scheme showing potential sites for secondary iodine addition on graphene forming all-*trans*-oligoene chains. The 1,2-, and *cis*-1,4 positions are precluded due to iodine atom size and I-I bond length (bottom right). C) Schematic illustration of the proposed iodinated graphene structure, explaining the observed Raman signals and doping properties. *Trans*-oligoene chains (red) with varying lengths and localized double bonds are embedded in graphene domains (grey) with a delocalized π-system. A The *cis*-1,4-addition is unlikely given the small I-I distance, despite the high spin density in this position. B Addition along a *trans*-1,4-oligoene chain ensures sufficient distance between iodine atoms. C Up to three *trans*-oligoene chains can extend from a single sp^3-defect, connecting to adjacent sp^3-defects across the graphene sheet. D Perfect zigzag edges separate the chains from graphene domains along the length of the chains. The delocalized double bonds have been omitted for clarity.

density (C, Figure 5C). The absence of a D-peak in the Raman spectra can be attributed to the perfect zigzag edges to the neighboring graphene domains (D, Figure 5C), rendering them Raman silent.[27,48] The polydisperse nature of iodinated graphene makes it impossible to give a definite structure since the patterns formed will be randomly distributed across the illuminated area and only a small part of the distribution is probed at a given laser wavelength matching the bandgap of the chains. As more and more radicals are added to the graphene sheet more conjugated double bonds become confined between defects and the uninterrupted graphene domains become smaller. The distribution of *trans*-oligoene chains will shift due to the decreasing defect distance, making long chains less likely.

3. Conclusion

In summary, defect-free graphene was functionalized by a photochemical iodination reaction for the first time and strong new Raman modes were observed. Thermal reversibility of the reaction, dispersion of Raman modes and complete disappearance of graphene Raman modes in some areas indicate the interaction of iodine with the graphene lattice carbon atoms. KPFM and transport measurements demonstrate the strong p-doping effect of iodinated graphene, exceeding non-covalent iodine doping. Due to the size of iodine atoms the usually observed 1,2- and *cis*-1,4-position addition patterns are sterically hindered, leading to regioselective functionalization of graphene, and generating *trans*-oligoene substructures. Those *trans*-oligoene structures generate new Raman modes by the isolation of conjugated double bonds between sp^3-defects. The proposed structure and reaction mechanism will serve as a starting point for further experimental and theoretical inquiries toward the rational design of regioselective patterning of graphene. The iodination-based functionalization approach paths a way to patterning applications accompanied with a strong p-doping effect and the ability of readout due to the strong Raman modes.

Supporting Information

Supporting Information is available from the Wiley Online Library or from the author.

Acknowledgements

S.E. and F.G. gratefully acknowledge funding from the Deutsche Forschungsgemeinschaft (DFG, German Research Foundation, Project No. 392444269).

Open access funding enabled and organized by Projekt DEAL.

Conflict of Interest

The authors declare no conflict of interest.

Data Availability Statement

The data that support the findings of this study are available in the supplementary material of this article.

Keywords

addition patterns, graphene, iodination, Raman spectroscopy, *trans*-oligoene

Received: December 21, 2023
Revised: February 6, 2024
Published online: March 20, 2024

[1] a) T. Wei, X. Liu, M. Kohring, S. Al-Fogra, M. Moritz, D. Hemmeter, U. Paap, C. Papp, H. P. Steinrück, J. Bachmann, H. B. Weber, F. Hauke, A. Hirsch, *Angew. Chem., Int. Ed.* **2022**, *61*, e202201169; b) M. Z. Hossain, M. B. A. Razak, H. Noritake, Y. Shiozawa, S. Yoshimoto, K. Mukai, T. Koitaya, J. Yoshinobu, S. Hosaka, *J. Phys. Chem. C* **2014**, *118*, 22096.

[2] C. Wetzl, A. Silvestri, M. Garrido, H. L. Hou, A. Criado, M. Prato, *Angew. Chem., Int. Ed.* **2023**, *62*, e202212857.

[3] G. Abellan, M. Schirowski, K. F. Edelthalhammer, M. Fickert, K. Werbach, H. Peterlik, F. Hauke, A. Hirsch, *J. Am. Chem. Soc.* **2017**, *139*, 5175.

[4] H. Qin, T. Hwang, C. Ahn, J. A. Kim, Y. Jin, Y. Cho, C. Shin, T. Kim, *J. Nanosci. Nanotechnol.* **2016**, *16*, 5034.
[5] M. Z. Hossain, J. E. Johns, K. H. Bevan, H. J. Karmel, Y. T. Liang, S. Yoshimoto, K. Mukai, T. Koitaya, J. Yoshinobu, M. Kawai, A. M. Lear, L. L. Kesmodel, S. L. Tait, M. C. Hersam, *Nat. Chem.* **2012**, *4*, 305.
[6] A. Criado, M. Melchionna, S. Marchesan, M. Prato, *Angew. Chem., Int. Ed.* **2015**, *54*, 10734.
[7] a) C. E. Halbig, R. Lasch, J. Krüll, A. S. Pirzer, Z. Wang, J. N. Kirchhof, K. I. Bolotin, M. R. Heinrich, S. Eigler, *Angew. Chem., Int. Ed.* **2019**, *58*, 3599; b) Y. Wang, F. Grote, Q. Cao, S. Eigler, *J. Phys. Chem. Lett.* **2021**, *12*, 10009.
[8] R. A. Schäfer, D. Dasler, U. Mundloch, F. Hauke, A. Hirsch, *J. Am. Chem. Soc.* **2016**, *138*, 1647.
[9] R. A. Borse, M. B. Kale, S. H. Sonawane, Y. Wang, *Adv. Funct. Mater.* **2022**, *32*, 2202570.
[10] F. Karlicky, K. Kumara Ramanatha Datta, M. Otyepka, R. Zboril, *ACS Nano* **2013**, *7*, 6434.
[11] a) P. Šimek, K. Klímová, D. Sedmidubský, O. Jankovský, M. Pumera, Z. Sofer, *Nanoscale* **2015**, *7*, 261; b) M. S. Mirshekarloo, M. C. D. Cooray, P. Jovanović, C. D. Easton, F. Wu, T. D. Gamot, M. J. Abedin, M. R. Yuce, M. Shaibani, M. Majumder, *Batter. Supercaps* **2021**, *4*, 1175; c) A. Wang, S. Bok, C. J. Mathai, K. Gangopadhyay, J. McFarland, M. R. Maschmann, S. Gangopadhyay, *Nano Futures* **2020**, *4*, 045002; d) X. Zhang, G. Lu, *Carbon* **2016**, *108*, 215.
[12] W. Li, Y. Li, K. Xu, *Nano Lett.* **2021**, *21*, 1150.
[13] L. Troian-Gautier, M. D. Turlington, S. A. M. Wehlin, A. B. Maurer, M. D. Brady, W. B. Swords, G. J. Meyer, *Chem. Rev.* **2019**, *119*, 4628.
[14] S. Niyogi, E. Bekyarova, J. Hong, S. Khizroev, C. Berger, W. de Heer, R. C. Haddon, *J. Phys. Chem. Lett.* **2011**, *2*, 2487.
[15] R. Balog, B. Jorgensen, J. Wells, E. Laegsgaard, P. Hofmann, F. Besenbacher, L. Hornekaer, *J. Am. Chem. Soc.* **2009**, *131*, 8744.
[16] J. M. Englert, C. Dotzer, G. Yang, M. Schmid, C. Papp, J. M. Gottfried, H. P. Steinrück, E. Spiecker, F. Hauke, A. Hirsch, *Nat. Chem.* **2011**, *3*, 279.
[17] a) V. Nagyte, D. J. Kelly, A. Felten, G. Picardi, Y. Shin, A. Alieva, R. E. Worsley, K. Parvez, S. Dehm, R. Krupke, S. J. Haigh, A. Oikonomou, A. J. Pollard, C. Casiraghi, *Nano Lett.* **2020**, *20*, 3411; b) Z. Wang, Q. Yao, C. Neumann, F. Börrnert, J. Renner, U. Kaiser, A. Turchanin, H. J. W. Zandvliet, S. Eigler, *Angew. Chem., Int. Ed.* **2020**, *59*, 13657.
[18] a) G. Copetti, E. H. Nunes, G. K. Rolim, G. V. Soares, S. A. Correa, D. E. Weibel, C. Radtke, *J. Phys. Chem. C* **2018**, *122*, 16333; b) Y. Rho, K. Lee, L. Wang, C. Ko, Y. Chen, P. Ci, J. Pei, A. Zettl, J. Wu, C. P. Grigoropoulos, *Nat. Electron.* **2022**, *5*, 505.
[19] H. González-Herrero, J. M. Gómez-Rodríguez, P. Mallet, M. Moaied, J. J. Palacios, C. Salgado, M. M. Ugeda, J. Y. Veuillen, F. Yndurain, I. Brihuega, *Science* **2016**, *352*, 437.
[20] a) I. A. Popov, Y. Li, Z. Chen, A. I. Boldyrev, *Phys. Chem. Chem. Phys.* **2013**, *15*, 6842; b) F. Marsusi, N. D. Drummond, M. J. Verstraete, *Carbon* **2019**, *144*, 615; c) P. A. Denis, *ChemPhysChem* **2013**, *14*, 3271.
[21] a) Z. Yao, H. Nie, Z. Yang, X. Zhou, Z. Liu, S. Huang, *Chem. Commun.* **2012**, *48*, 1027; b) N. Jung, A. C. Crowther, N. Kim, P. Kim, L. Brus, *ACS Nano* **2010**, *4*, 7005.
[22] N. Jung, N. Kim, S. Jockusch, N. J. Turro, P. Kim, L. Brus, *Nano Lett.* **2009**, *9*, 4133.
[23] J. M. Gardner, M. Abrahamsson, B. H. Farnum, G. J. Meyer, *J. Am. Chem. Soc.* **2009**, *131*, 16206.
[24] B. Li, L. Zhou, D. Wu, H. Peng, K. Yan, Y. Zhou, Z. Liu, *ACS Nano* **2011**, *5*, 5957.
[25] P. H. Svensson, L. Kloo, *Chem. Rev.* **2003**, *103*, 1649.
[26] J. M. Englert, P. Vecera, K. C. Knirsch, R. A. Schäfer, F. Hauke, A. Hirsch, *ACS Nano* **2013**, *7*, 5472.
[27] A. C. Ferrari, D. M. Basko, *Nat. Nanotechnol.* **2013**, *8*, 235.
[28] M. Tasumi, H. Yoshida, M. Fujiwara, H. Hamaguchi, H. Shirakawa, *Synth. Met.* **1987**, *17*, 319.
[29] V. Rives-Arnau, N. Sheppard, *J. Chem. Soc., Faraday Trans.* **1980**, *76*, 394.
[30] A. C. Ferrari, J. Robertson, *Phys. Rev. B* **2001**, *63*, 075414.
[31] a) H. E. Schaffer, R. R. Chance, R. J. Silbey, K. Knoll, R. R. Schrock, *J. Chem. Phys.* **1991**, *94*, 4161; b) K. Furuya, A. Sakamoto, M. Tasumi, *J. Phys. Chem. A* **2023**, *127*, 5344.
[32] A. C. Ferrari, J. Robertson, *Phys. Rev. B* **2000**, *61*, 14095.
[33] J. Hong, M. K. Park, E. J. Lee, D. Lee, D. S. Hwang, S. Ryu, *Sci. Rep.* **2013**, *3*, 2700.
[34] X. Tang, T. Fan, C. Wang, H. Zhang, *Small* **2021**, *17*, e2005640.
[35] O. Jankovsky, P. Simek, K. Klimova, D. Sedmidubsky, S. Matejkova, M. Pumera, Z. Sofer, *Nanoscale* **2014**, *6*, 6065.
[36] Z. Wang, Q. Yao, Y. Hu, C. Li, M. Hussmann, B. Weintrub, J. N. Kirchhof, K. Bolotin, T. Taniguchi, K. Watanabe, S. Eigler, *RSC Adv.* **2019**, *9*, 38011.
[37] S. W. Chu, S. J. Baek, D. C. Kim, S. Seo, J. S. Kim, Y. W. Park, *Synth. Met.* **2012**, *162*, 1689.
[38] a) H. Wang, Y. Wu, C. Cong, J. Shang, T. Yu, *ACS Nano* **2010**, *4*, 7221; b) T. S. Sreeprasad, V. Berry, *Small* **2013**, *9*, 341.
[39] a) X. Zhang, A. Hsu, H. Wang, Y. Song, J. Kong, M. S. Dresselhaus, T. Palacios, *ACS Nano* **2013**, *7*, 7262; b) L. Zhou, L. Zhou, M. Yang, D. Wu, L. Liao, K. Yan, Q. Xie, Z. Liu, H. Peng, Z. Liu, *Small* **2013**, *9*, 1388.
[40] A. M. Goossens, V. E. Calado, A. Barreiro, K. Watanabe, T. Taniguchi, L. M. K. Vandersypen, *Appl. Phys. Lett.* **2012**, *100*, 073110 .
[41] N. Jung, B. Kim, A. C. Crowther, N. Kim, C. Nuckolls, L. Brus, *ACS Nano* **2011**, *5*, 5708.
[42] C. Horie, M. Maeda, Y. Kuramoto, *Physica B+C* **1980**, *99*, 430.
[43] a) L. Bao, B. Zhao, B. Yang, M. Halik, F. Hauke, A. Hirsch, *Adv. Mater.* **2021**, *33*, 2101653; b) T. Wei, M. Kohring, H. B. Weber, F. Hauke, A. Hirsch, *Nat. Commun.* **2021**, *12*, 552; c) M. Yang, L. Zhou, J. Wang, Z. Liu, Z. Liu, *J. Phys. Chem. C* **2011**, *116*, 844.
[44] D. E. Jiang, B. G. Sumpter, S. Dai, *J. Phys. Chem. B* **2006**, *110*, 23628.
[45] P. Ruffieux, O. Groning, P. Schwaller, L. Schlapbach, P. Groning, *Phys. Rev. Lett.* **2000**, *84*, 4910.
[46] O. V. Yazyev, L. Helm, *Phys. Rev. B* **2007**, *75*, 125408.
[47] C. Castiglioni, M. Tommasini, G. Zerbi, *Philos. Trans. R. Soc. A* **2004**, *362*, 2425.
[48] C. Casiraghi, A. Hartschuh, H. Qian, S. Piscanec, C. Georgi, A. Fasoli, K. S. Novoselov, D. M. Basko, A. C. Ferrari, *Nano Lett.* **2009**, *9*, 1433.